CHINESE OPTICS LETTERS

Vol. 20, No. 10 | October 2022

Delivery of 40 Gbit/s W-band signal over 4600 m wireless distance employing advanced digital signal processing

Bowen Zhu (朱博文), Yanyi Wang (王演祎), Weiping Li (李韦萍), Feng Wang (王 峰), Jiaxuan Liu (刘家轩), Miao Kong (孔 淼), and Jianjun Yu (余建军)*

Key Laboratory for Information Science of Electromagnetic Waves (MoE), Fudan University, Shanghai 200433, China

*Corresponding author: jianjun@fudan.edu.cn

Received March 7, 2022 | Accepted May 25, 2022 | Posted Online June 25, 2022

We experimentally built a photonics-aided long-distance large-capacity millimeter-wave wireless transmission system and demonstrated a delivery of 40 Gbit/s W-band 16-ary quadrature amplitude modulation (QAM) signal over 4600 m wireless distance at 88.5 GHz. Advanced offline digital signal processing algorithms are proposed and employed for signal recovery, which makes the bit-error ratio under 2.4×10^{-2}. To the best of our knowledge, this is the first field-trial demonstration of $>$4 km W-band 16QAM signal transmission, and the result achieves a record-breaking product of wireless transmission capacity and distance, i.e., 184 (Gbit/s)·km, for high-speed and long-distance W-band wireless communication.

Keywords: millimeter-wave communication; digital signal processing; W-band; photonics-aided technique.

DOI: 10.3788/COL202220.103901

1. Introduction

Due to the explosive growth of mobile data traffic, the spectrum resources of sub-6-GHz have become increasingly crowded. In recent years, millimeter-wave (mm-wave) wireless communications, which can provide larger bandwidths, have received much attention because of their higher carrier frequencies (30–300 GHz). Among them, the W-band (75–110 GHz) can support broadband communication up to 35 GHz and has low atmospheric attenuation ($< 0.5\,\mathrm{dB/km}$) with good directionality, which is very suitable for large-capacity, long-distance wireless transmission. In addition, high-speed long-distance point-to-point W-band wireless links can also replace the fiber links for wireless cellular base stations backhaul, as an alternative deployed in special terrain areas, where it is difficult to lay optical cables, or as an emergency plan to deal with communication interruptions caused by sudden natural disasters. Generally, due to the limitation of electronic components, it is very difficult to generate high-frequency mm-wave radio frequency (RF) signals based on pure electric ways, while the photonics-aided mm-wave generation technique can overcome the bandwidth limitation of electronic components and be easily deployed in fiber-wireless integrated systems for the seamless connection between fiber networks and wireless networks[1–5]. There are many mm-wave generation techniques using novel optical sources that have been proposed[6–13].

As can be seen, many large-capacity photonics-aided W-band mm-wave signal transmission results have been reported recently[14–19]. With the comprehensive use of multiple multi-dimensional multiplexing techniques, such as high-order modulation format, optical polarization multiplexing, antenna polarization multiplexing, and line-of-sight (LOS) multi-input multi-output (MIMO), the transmission rate can reach more than 100 Gbit/s, or even 400 Gbit/s. However, most of these experiments are restricted indoor with short wireless distance, and few of them demonstrate field-trial transmission beyond 1 km. Figure 1 summarizes a series of experimental demonstrations[20–24] that we have successfully achieved in the past on photonics-aided W-band mm-wave signal transmission over long wireless distances ($\geq 100\,\mathrm{m}$) and clearly indicates the carrier frequency, the achieved data rate, the delivered wireless distance, and the detailed signal modulation format for each transmission. Notably, in Ref. [23], a 20 Gbit/s photonics-aided W-band quadrature phase-shift keying (QPSK) signal delivery over 1.7 km wireless distance at 94 GHz is reported, and Ref. [24] achieves the product of wireless transmission capacity and distance of $54\,\mathrm{Gbit/s} \times 2.5\,\mathrm{km} = 135\,(\mathrm{Gbit/s}) \cdot \mathrm{km}$ at the 90 GHz W-band employing optical polarization multiplexing and antenna polarization multiplexing techniques together, which is the best experimental result so far.

In this Letter, the delivery of a 10 Gbaud 16-ary quadrature amplitude modulation (QAM) W-band signal over 4600 m is demonstrated experimentally, based on a high-speed and long-wireless-distance photonics-aided mm-wave system. At the same time, we also try and discuss advanced digital signal processing (DSP) algorithms for signal recovery at the receiver, such as flexible carrier phase recovery (CPR) algorithms and nonlinear equalizers, to obtain better system performance. To the best of our knowledge, the corresponding product of wireless

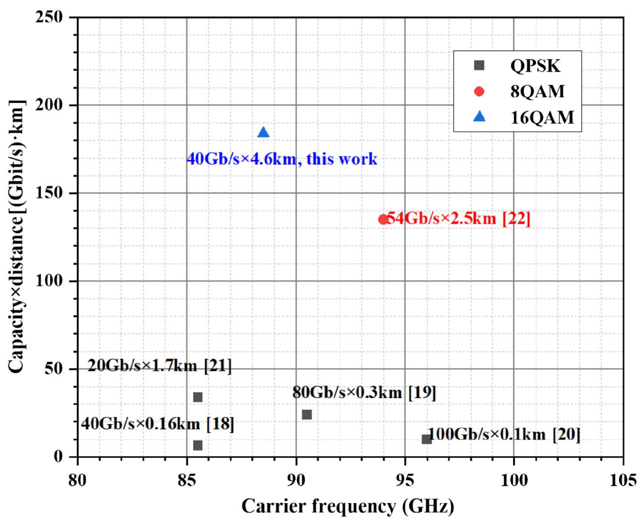

Fig. 1. Our experimental demonstrations on photonics-aided W-band mm-wave signal transmission over long wireless distance (≥100 m).

transmission capacity and distance, i.e., 184 (Gbit/s)·km, is a record-breaking result for high-speed and long-distance W-band wireless communication.

2. Experimental Setup and Advanced DSP Algorithms

The entire experimental setup is shown in Fig. 2. At the optical transmitter, two tunable external cavity lasers (ECLs) with linewidth less than 100 kHz emit two continuous waves (CWs) as an optical local oscillator (LO) and for signal modulation, respectively. The frequency spacing of the CWs is set at approximately 88.5 GHz to generate the RF signal at the corresponding carrier frequency by means of optical beating. Considering that the emission frequencies of lasers are not locked, the frequency offset recovery algorithm in the offline DSP is necessary. The electrical signals output by an arbitrary waveform generator (AWG) are amplified by two parallel electrical amplifiers (EAs) and then fed into an in-phase and quadrature (I/Q) modulator with 25 GHz bandwidth for electrical-to-optical conversion to generate the optical QAM signal. After the insertion loss and modulation loss are compensated by the polarization-maintaining erbium-doped fiber amplifier (PM-EDFA), the signal and the optical LO with the same power (13 dBm) are coupled by a polarization-maintaining optical coupler (PM-OC). As depicted in Fig. 3(a), the optical transmitter is placed indoors. After the fronthaul over 100 m standard single-mode fiber, the optical signal and LO are converted to a W-band mm-wave by a 100 GHz single-ended photodiode (PD).

The wireless transmitter and receiver are located on two roofs 4.6 km apart between the two campuses of Fudan University, as shown in Fig. 3(b). Note that there is also a vertical height difference of about 120 m between the wireless transmitter and receiver. The mm-wave RF signal is boosted by a W-band low-noise amplifier (LNA) with 30 dB gain and W-band power amplifiers (PAs) with 18 dBm saturation output power. The wireless signals are transmitted and received by means of a pair of horn antennas (HAs) with 25 dBi gain working at the W-band, and the 3 dB beam width is about 10° for the E-plane and 10.5° for the H-plane at 88.5 GHz. It is worth noting that the addition of two lenses in front of the HAs increases the antenna gain G_T to 34 dBi and G_R to 54 dBi. The position of the lenses has been tested in advance for optimum gain. Based on the Friis transmission equation, we can estimate the wireless received power as[25]

$$P_R(\mathrm{dBm}) = P_T + G_T - 20\log\left(\frac{4\pi d}{\lambda}\right) - L_A \times d + G_R, \qquad (1)$$

where P_T denotes the wireless transmitted power, λ denotes the carrier operating wavelength of the wireless link, d denotes the wireless distance, and L_A denotes the atmospheric loss factor, which is determined by weather conditions.

In our experiment, considering that the free space path loss of the W-band signal at 88.5 GHz (λ is ~3.39 mm) is about 144.6 dB after 4600 m wireless transmission, and L_A is about

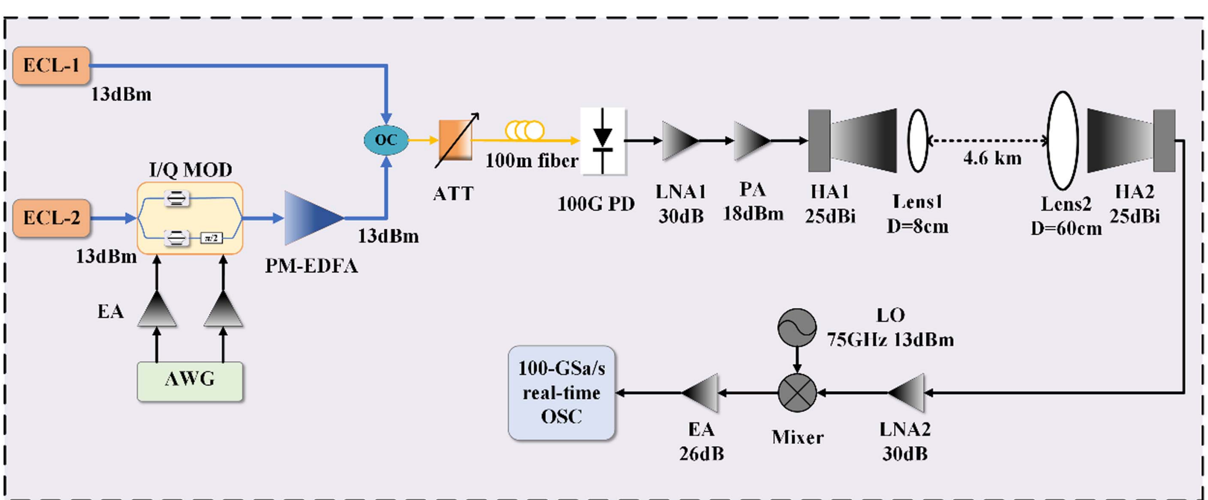

Fig. 2. Experimental setup of the photonics-aided W-band mm-wave signal transmission system.

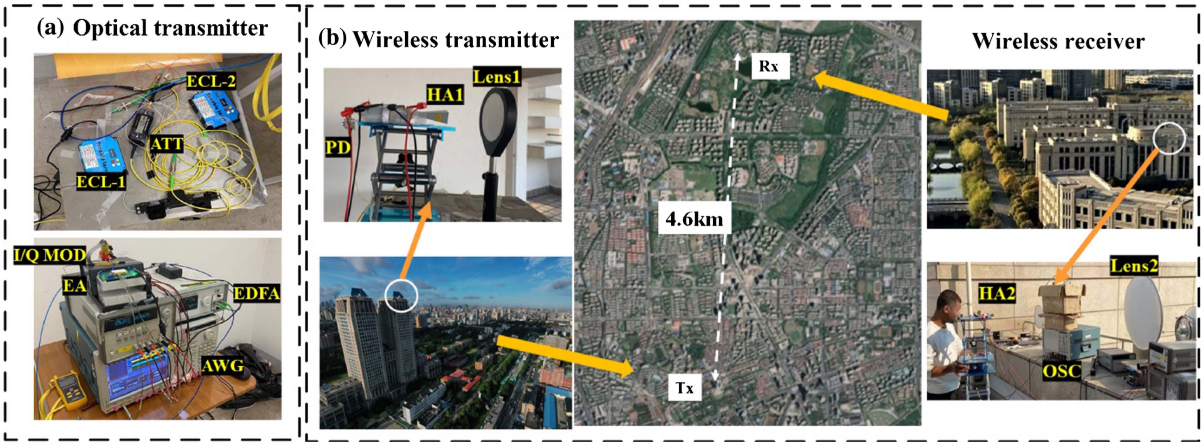

Fig. 3. (a) Photos of the optical transmitter indoors; (b) satellite map display of 4600 m wireless transmission link and the photos of the wireless transmitter and receiver.

0.5 dB/km at the W-band on a sunny day[26], when the wireless transmitted power is 16 dBm, the received power after HA is calculated as $16 + 34 - 144.6 + 54 - 0.5 \times 4.6 = -42.9\,\text{dBm}$, which is very close to our measured value of −43.1 dBm. The small gap between theoretical and measured values may be due to other factors, such as the additional power loss caused by the devices' connection.

At the receiver end, the signal is firstly boosted by a W-band LNA and then down-converted to an intermediate frequency (IF) signal at 13.5 GHz with a mixer driven by a 75 GHz electrical LO. Finally, the signal is amplified by an EA with 26 dB gain and captured at 100 GSa/s by a real-time oscilloscope (OSC) with 33 GHz bandwidth.

The offline DSPs include down-conversion to baseband, resampling, T/2-spaced constant-modulus algorithm (CMA) for coarse equalization, frequency offset recovery, CPR, 171 tap T-spaced direct-detection least mean square (DD-LMS) for fine equalization and advanced nonlinear equalization, as shown in Fig. 4(a).

Considering the complexity and performance under different received signal power, two algorithms, blind phase search (BPS) and principal component-based phase estimation (PCPE)[27], are flexibly selected for CPR. In general, BPS is a classical algorithm for CPR of higher-order M-QAM constellations, which is suitable for parallel implementations and has been shown to have excellent performance. However, PCPE is a more robust CPR algorithm for the high-power signals distorted by saturation, as well as the probabilistic-shaped (PS)[28] QAM signals. This is because the BPS algorithm relies on blind search and decision operation to test the phase. If the constellation points of the outer ring are squeezed together, or the probability of occurrence is very low, it may lead to serious errors in the decision operation of the BPS algorithm. The PCPE algorithm only extracts the principal components of the squared QAM constellation and does not involve the decision operation of a single constellation point. Compared with other optical communication systems, the nonlinear saturation effect caused by high-power signal injection into the optical/electrical (O/E) devices is more significant in our mm-wave systems, so PCPE is a good choice to replace BPS at this time. The flow of the PCPE algorithm is shown in Fig. 4(b).

In our experimental system, the unequal drive amplitude before the modulator and the wrong offset point of the $\pi/2$ phase shifter in the optical I/Q modulator, as well as the imperfection of the electrical mixer at the receiver, will bring about the I/Q amplitude or phase imbalance. Moreover, the timing skew between I/Q channels may lead to I/Q skew. These problems will seriously degrade the performance of the system. We

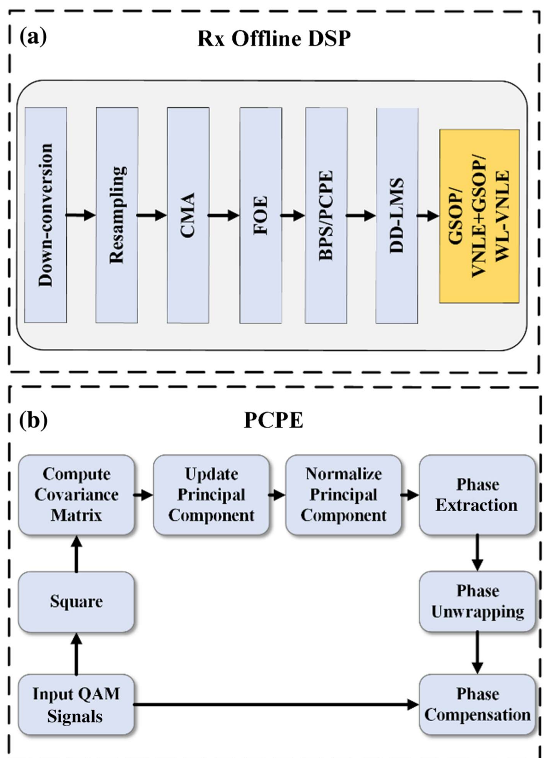

Fig. 4. (a) Block diagram of the offline DSPs for signal recovery; (b) block diagram of PCPE algorithm.

commonly use the Gram–Schmidt orthogonalization process (GSOP) algorithm to mitigate the I/Q imbalance and I/Q skew in the digital coherent optical systems. The computational complexity of the GSOP algorithm is low, but it is hard to completely correct the IQ-distorted QAM constellation.

Regarding the nonlinear compensation for O/E components in optical communication, it has not yet been formulated as a standard in actual products, but it has been widely discussed in research. However, at the technological edge of high-speed transmission, nonlinear compensation will be extremely important. The Volterra nonlinear equalizer (VNLE) based on the principle of the Volterra series can realize nonlinear compensation of the received signal by fitting separately from low-order to high-order. In general, a third-order VNLE is sufficient to overcome most nonlinear effects in the system and keep the computational complexity from being too bulky. The fundamental formula of a third-order VNLE can be expressed as[29]

$$y(n)=\sum_{i=0}^{L-1}h_1(i)x(n-i)+\sum_{i=0}^{N-1}\sum_{j=0}^{i}h_2(i,j)x(n-i)x(n-j)+\sum_{i=0}^{M-1}\sum_{j=0}^{i}\sum_{k=0}^{j}h_3(i,j,k)x(n-i)x(n-j)x(n-k), \tag{2}$$

where L, N, and M represent the first, second, and third-order tap numbers, respectively.

Here, we propose and apply a novel widely linear and VNLE (WL-VNLE) in the experiment to address the I/Q and nonlinear effects of the signal simultaneously, which can be expressed as

$$y(n)=\sum_{i=0}^{L-1}h_1(i)x(n-i)+\sum_{i=0}^{L-1}h_{1^*}(i)x^*(n-i)+\sum_{i=0}^{N-1}\sum_{j=0}^{i}h_2(i,j)x(n-i)x(n-j)+\sum_{i=0}^{M-1}\sum_{j=0}^{i}\sum_{k=0}^{j}h_3(i,j,k)x(n-i)x(n-j)x(n-k), \tag{3}$$

where $[\cdot]^*$ means complex conjugate operation. The nonlinear parts of the equalizer are unchanged, while the linear part is expanded to input the signal and its complex conjugate together. This extra part in the equation can effectively correct the I/Q misalignment.

3. Experimental Results and Discussions

Figure 5 shows the bit-error ratio (BER) versus input optical power into the PD for the 10 Gbaud QPSK signal, as well as the constellation diagrams under different algorithms at −2 dBm. Since the QPSK modulation has only four signal positions, the influence of the I/Q mixing effect on the received constellation and the performance of different correction algorithms can be clearly perceived. When neither GSOP nor VNLE algorithms are used, the received constellation has significant skew compared to the standard QPSK constellation diagram. VNLE can

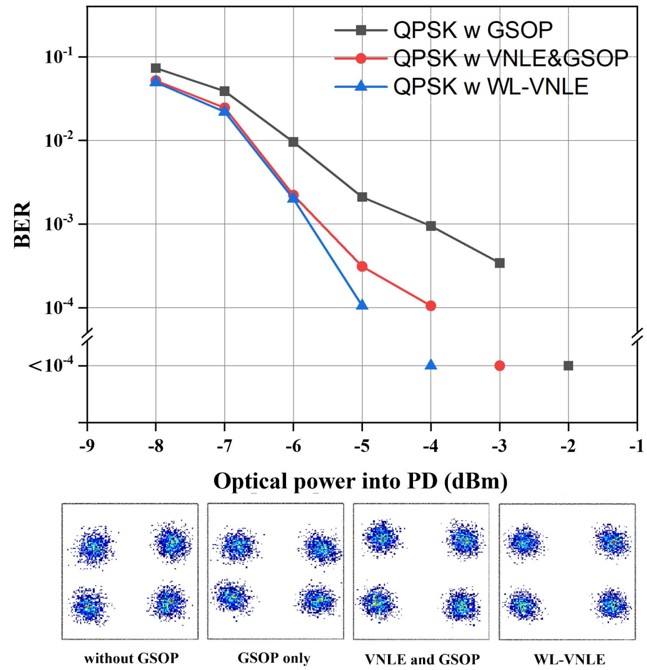

Fig. 5. BER versus input optical power into PD for 10 Gbaud QPSK signal and the constellation diagrams under different algorithms at -2 dBm.

further overcome nonlinear effects in the system, which makes the constellation points appear more convergent. A very intuitive conclusion is that the performance of VNLE/WL-VNLE becomes better as the optical power of the input PD increases, which is due to the positive correlation between the channel nonlinear response and the input power. VNLE can bring a sensitivity gain of ~0.5 dB at the 20% soft decision forward-error-correction (SD-FEC) threshold of 2.4×10^{-2}. After using WL-VNLE, the I/Q imbalance and I/Q skew are better corrected, compared to cascading VNLE and GSOP. We can obtain a pre-FEC BER below 10^{-4} by WL-VNLE for a 10 Gbaud QPSK signal with input power more than −4 dBm.

The results for the 10 Gbaud 16QAM signal and the constellation diagrams under different algorithms at −2 dBm are shown in Fig. 6. When the input power is larger, the 16QAM signal suffers from more nonlinear distortion, which is mainly due to the saturation effects of the LNA and PA in the wireless transmitter. While 16QAM is a high-order modulation format, its constellation is more affected by device saturation effects than QPSK. The BER performance begins to degrade after the input power increases to greater than −2 dBm. This is a trade-off for getting a higher SNR or suffering from less nonlinear distortion. At input powers of −1 dBm and 0 dBm, the BPS algorithm cannot even successfully estimate the phase noise due to the squeezing and deformation of the inner and outer constellation points. In this situation, the PCPE algorithm can work without problems, and CPR is achieved. Furthermore, VNLE greatly alleviates the nonlinear distortion in the experimental system, allowing the BER to reach under the 20% SD-FEC threshold. WL-VNLE can bring an additional sensitivity gain of ~0.5 dB, compared to cascading VNLE and GSOP.

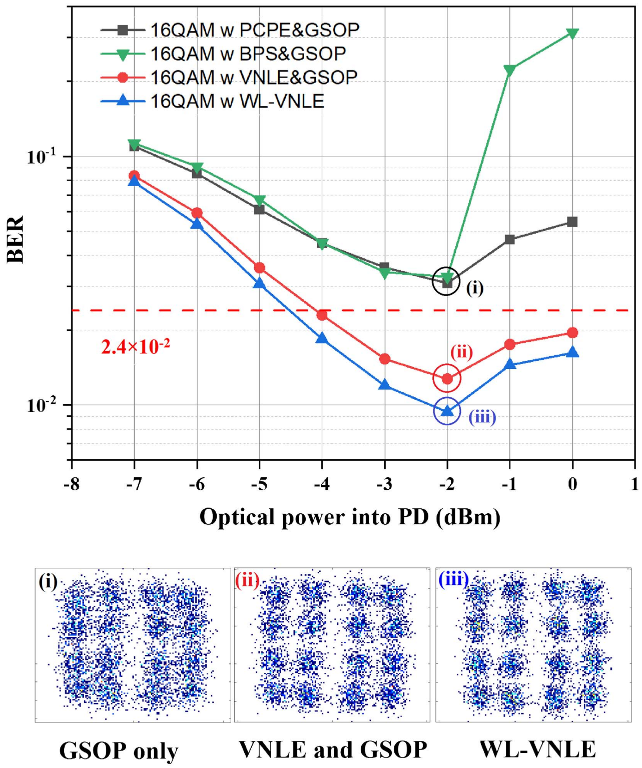

Fig. 6. BER versus input optical power into the PD for 10 Gbaud 16QAM signal and the constellation diagrams under different algorithms at −2 dBm.

The transmission performance at different carrier frequencies is also tested and presented in Fig. 7(a). For photonics-aided mm-wave generation systems, this is easily achieved by simply tuning the operating wavelength of the ECLs. As the IF increases from 13.5 GHz to 20.2 GHz (carrier frequency from 88.5 GHz to 95.2 GHz), the performance of the 10 Gbaud PS-16QAM signal generally tends to decrease. As shown in Figs. 7(b) and 7(c), signal fading is more serious in the receiving spectrum when the IF is 20.2 GHz rather than 13.5 GHz. In the high-frequency region beyond 98 GHz, the signal spectrum is almost overwhelmed by noise because the carrier frequency deviates from the optimal response range of the devices.

Due to the limitations of devices and experimental conditions, it is difficult to experimentally explore the potential transmission performance of the photonic mm-wave system. Therefore, under the premise of restoring the real experimental parameters as much as possible, we conducted a virtual photonics integrated (VPI) simulation of the entire transmission system.

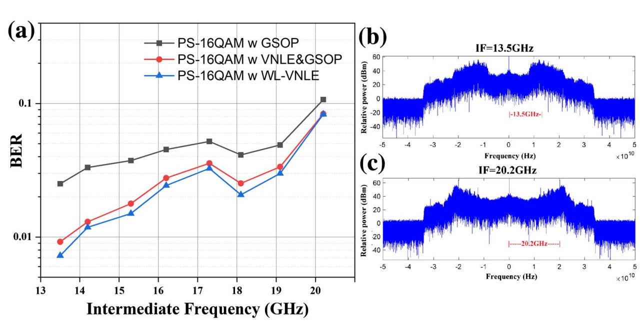

Fig. 7. (a) BER versus IF for 10 Gbaud PS-16QAM signal at −3 dBm; (b), (c) electrical spectrum of received signal at IF 13.5 GHz and 20.2 GHz.

Figure 8 shows the results of 16QAM signal performance with higher baud rates. Since the simulation does not involve the I/Q mixing effects and nonlinear saturation effects, the corresponding compensation algorithms are not applied. All results in the figure are measured with the input optical power at −2 dBm and carrier frequency at 88.5 GHz. The two curves on the figure estimate the effect of the PA frequency response on transmission performance under experimental conditions and under more ideal conditions, respectively. If the 3 dB bandwidth of the PA is only set to 10 GHz (similar to that used in the experiment), the maximum baud rate that can be tolerated under the SD-FEC threshold is less than 15 Gbaud, and the total rate is less than 60 Gbit/s. When the frequency response of the PA is more ideal, the system has a potential transmission capacity of more than

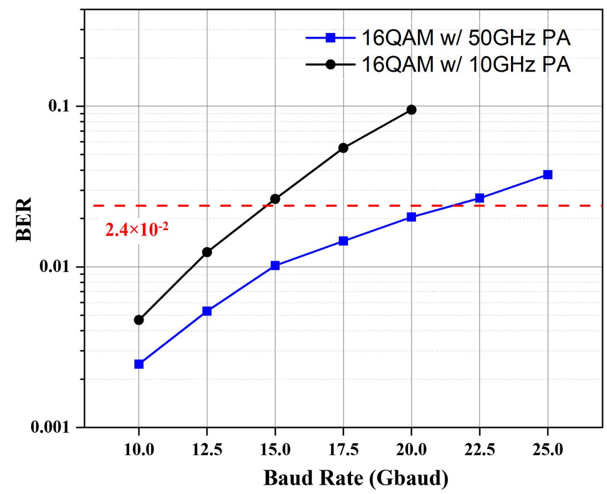

Fig. 8. Simulation results of 16QAM signal transmission over 4600 m with higher baud rates.

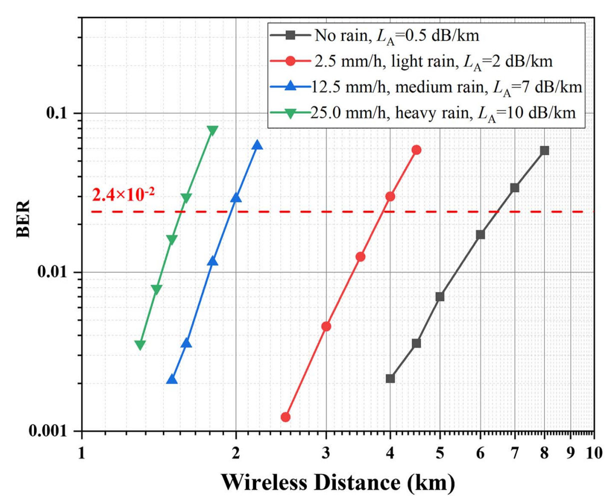

Fig. 9. Simulation results of 10 Gbaud 16QAM signal transmission in different weather.

80 Gbit/s, and the limitation at this time mainly comes from the PD.

Finally, the maximum transmission distances of the 10 Gbaud 16QAM signal are estimated by simulation in different weather[30], as shown in Fig. 9. When the rainfall reaches 25 mm/h, the parameter L_A in Eq. (1) will increase to 10 dB/km, which makes the wireless transmission distance limited within 1600 m. While on a sunny day, like our experimental condition, the maximum wireless distance that a 40 Gbit/s signal can transmit is expected to exceed 6500 m. In light rain, the system still has a long-distance transmission potential of nearly 4000 m.

4. Conclusion

We experimentally demonstrated a 10 Gbaud 16QAM photonics-aided W-band mm-wave signal transmission over 4600 m wireless distance. With the help of the proposed WL-VNLE algorithm, the total rate reaches 40 Gbit/s with BER below the 20% SD-FEC threshold of 2.4×10^{-2}, and a record-breaking product of wireless transmission capacity and distance up to 184 (Gbit/s)·km is achieved. By further simulation, it is foreseeable that the single-channel data rate of the photonics-aided W-band transmission system is promising close to 100 Gbit/s, even after long-distance transmission. The maximum wireless transmission distance is expected to exceed 6500 m for the 40 Gbit/s signal. The experiments fully verify the potential of photonics-aided W-band mm-wave for large-capacity and long-distance wireless transmission.

Acknowledgement

This work was partially supported by the National Key R&D Program of China (No. 2018YFB1800905) and the National Natural Science Foundation of China (Nos. 61935005, 91938202, 61720106015, 61835002, 62127802, and 61805043).

References

1. P. T. Dat, A. Kanno, T. Umezawa, N. Yamamoto, and T. Kawanishi, "Millimeter-and terahertz-wave radio-over-fiber for 5G and beyond," in *IEEE Photonics Society Summer Topical Meeting Series (SUM)* (2017), p. 165.
2. X. Li, J. Yu, and G.-K. Chang, "Photonics-aided millimeter-wave technologies for extreme mobile broadband communications in 5G," J. Light. Technol. **38**, 366 (2019).
3. J. Yu, "Photonics-assisted millimeter-wave wireless communication," IEEE J. Quantum Electron. **53**, 8000517 (2017).
4. J. Yu, X. Li, and W. Zhou, "Tutorial: broadband fiber-wireless integration for 5G+ communication," APL Photonics **3**, 111101 (2018).
5. X. Li, Z. Dong, J. Yu, N. Chi, Y. Shao, and G. K. Chang, "Demonstration of ultra-high bit rate fiber wireless transmission system of 108-Gb/s data over 80-km fiber and 2 × 2 MIMO wireless links at 100 GHz W-band frequency," in *Optical Fiber Communication Conference* (2013), paper JW2A. 75.
6. K. Mallick, P. Mandal, R. Mukherjee, G. C. Mandal, B. Das, and A. S. Patra, "Generation of 40 GHz/80 GHz OFDM based MMW source and the OFDM-FSO transport system based on special fine tracking technology," Opt. Fiber Technol. **54**, 102130 (2020).
7. G. C. Mandal, R. Mukherjee, B. Das, and A. S. Patra, "A full-duplex WDM hybrid fiber-wired/fiber-wireless/fiber-VLC/fiber-IVLC transmission system based on a self-injection locked quantum dash laser and a RSOA," Opt. Commun. **427**, 202 (2018).
8. M. Z. M. Khan, "Quantum-dash laser-based tunable 50/75 GHz mmW transport system for future L-band networks," IEEE Photon. Technol. Lett. (2022).
9. Q. Tareq, A. M. Ragheb, M. A. Esmail, S. A. Alshebeili, and M. Z. M. Khan, "Performance of injection-locked quantum-dash MMW source under clear and dusty weather conditions," IEEE Photonics J. **13**, 1500409 (2021).
10. P. T. Dat, Y. Yamaguchi, M. Motoya, S. Oikawa, J. Ichikawa, A. Kanno, N. Yamamoto, and T. Kawanishi, "Transparent fibermillimeter-wavefiber system in 100-GHz band using optical modulator and photonic down-conversion," J. Light. Technol. **40**, 1483 (2022).
11. Z.-K. Weng, Y.-C. Chi, H.-Y. Wang, C.-T. Tsai, C.-H. Cheng, and G.-R. Lin, "100-km long-reach carrierless 5G MMWoF link with destructive-interference-beating or single-sideband-filtering OFDM," J. Light. Technol. **39**, 7831 (2021).
12. Y. Wang, K. Wang, W. Zhou, and J. Yu, "Photonic aided vector millimeter-wave signal generation without digital-to-analog converter," Chin. Opt. Lett. **19**, 011101 (2021).
13. F. Zhao, J. Yu, and J. Li, "Dual-services generation using an integrated polarization multiplexing modulator," Chin. Opt. Lett. **18**, 110601 (2020).
14. X. Li, J. Yu, J. Zhang, F. Li, and J. Xiao, "Antenna polarization diversity for 146 Gb/s polarization multiplexing QPSK wireless signal delivery at W-band," in *Optical Fiber Communication Conference* (2014), paper M3D. 7.
15. J. Zhang, J. Yu, N. Chi, Z. Dong, X. Li, and G.-K. Chang, "Multichannel 120-Gb/s data transmission over 2 × 2 MIMO fiber-wireless link at W-band," IEEE Photon. Technol. Lett. **25**, 780 (2013).
16. X. Li, J. Yu, J. Xiao, and Y. Xu, "Fiber-wireless-fiber link for 128-Gb/s PDM-16QAM signal transmission at W-band," IEEE Photon. Technol. Lett. **26**, 1948 (2014).
17. X. Li, J. Yu, J. Zhang, Z. Dong, F. Li, and N. Chi, "A 400G optical wireless integration delivery system," Opt. Express **21**, 18812 (2013).
18. J. Yu, X. Li, J. Zhang, and J. Xiao, "432-Gb/s PDM-16QAM signal wireless delivery at W-band using optical and antenna polarization multiplexing," in *European Conference on Optical Communication (ECOC)* (2014), p. 1.
19. X. Pang, A. Caballero, A. Dogadaev, V. Arlunno, R. Borkowski, J. S. Pedersen, L. Deng, F. Karinou, F. Roubeau, and D. Zibar, "100 Gbit/s hybrid optical fiber-wireless link in the W-band (75–110 GHz)," Opt. Express **19**, 24944 (2011).
20. J. Xiao, J. Yu, X. Li, Y. Xu, Z. Zhang, and L. Chen, "40-Gb/s PDM-QPSK signal transmission over 160-m wireless distance at W-band," Opt. Lett. **40**, 998 (2015).
21. X. Li, J. Yu, J. Xiao, Z. Zhang, Y. Xu, and L. Chen, "Field trial of 80-Gb/s PDM-QPSK signal delivery over 300-m wireless distance with MIMO and antenna polarization multiplexing at W-band," in *Optical Fiber Communication Conference* (2015), paper Th5A. 5.
22. X. Li, J. Yu, and J. Xiao, "1003 (100 Gb/s × 100 m × 100 GHz) optical wireless system," in *European Conference on Optical Communication (ECOC)* (2015), p. 1.
23. J. Xiao, J. Yu, X. Li, Y. Xu, Z. Zhang, and L. Chen, "20-Gb/s PDM-QPSK signal delivery over 1.7-km wireless distance at W-band," in *Optical Fiber Communication Conference* (2015), paper W4G. 4.
24. X. Li, J. Yu, K. Wang, Y. Xu, L. Chen, L. Zhao, and W. Zhou, "Bidirectional delivery of 54-Gbps 8QAM W-band signal and 32-Gbps 16QAM K-band signal over 20-km SMF-28 and 2500-m wireless distance," in *Optical Fiber Communication Conference* (2017), paper Th5A. 7.
25. H. T. Friis, "A note on a simple transmission formula," Proc. IRE **34**, 254 (1946).
26. P Series, "Attenuation by atmospheric gases and related effects," Recommendation ITU-R (2019), p. 676.
27. J. C. M. Diniz, Q. Fan, S. M. Ranzini, F. N. Khan, F. Da Ros, D. Zibar, and A. P. T. Lau, "Low-complexity carrier phase recovery based on principal component analysis for square-QAM modulation formats," Opt. Express **27**, 15617 (2019).
28. L. Schmalen, "Probabilistic constellation shaping: challenges and opportunities for forward error correction," in *Optical Fiber Communication Conference* (2018), paper M3C. 1.
29. C. Bluemm, M. Schaedler, M. Kuschnerov, F. Pittalà, and C. Xie, "Single carrier vs. OFDM for coherent 600 Gb/s data centre interconnects with nonlinear equalization," in *Optical Fiber Communication Conference* (2019), paper M3H. 3.
30. Á. Faragó, P. Kántor, and J. Z. Bitó, "Rain effects on 5G millimeter wave ad-hoc mesh networks investigated with different rain models," Period. Polytech. Electr. Eng. Comput. Sci. **60**, 44 (2016).